HHS Public Access

Author manuscript

Eur Radiol. Author manuscript; available in PMC 2023 July 01.

Published in final edited form as:

Eur Radiol. 2022 July ; 32(7): 4967–4979. doi:10.1007/s00330-021-08529-x.

Diagnostic Accuracy of 2-[^{18}F]FDG-PET and Whole-Body DW-MRI for The Detection of Bone Marrow Metastases in Children and Young Adults

Ali Rashidi[1],

Lucia Baratto[1],

Ashok Joseph Theruvath[1],

Elton Benjamin Greene[2],

K Elizabeth Hawk[1],

Rong Lu[3],

Michael P. Link[4],

Sheri L. Spunt[4],

Heike E. Daldrup-Link[1,4]

[1]Department of Radiology, Molecular Imaging Program at Stanford, Stanford University School of Medicine, Stanford, CA, USA

[2]Department of Radiology, Pediatric Radiology, Lucile Packard Children's Hospital, Stanford University School of Medicine, Stanford, CA, USA

[3]Quantitative Sciences Unit, School of Medicine, Stanford University, Stanford, CA, USA

[4]Department of Pediatrics, Hematology/Oncology, Stanford University School of Medicine, Stanford, CA, USA

Abstract

Objectives: To compare the diagnostic accuracy of 2-[^{18}F]fluoro-2-deoxy-D-glucose enhanced positron emission tomography (2-[^{18}F]FDG-PET) and diffusion-weighted magnetic resonance imaging (DW-MRI) for the detection of bone marrow metastases in children and young adults with solid malignancies.

Methods: In this cross-sectional single-center institutional review board-approved study, we investigated twenty-three children and young adults (mean age, 16.8 years +/− 5.1 [standard deviation]; age range, 7–25 years; 16 males, 7 females) with 925 bone marrow metastases who underwent 66 simultaneous 2-[^{18}F]FDG-PET and DW-MRI scans including 23 baseline scans and 43 follow-up scans after chemotherapy between May 2015 and July 2020. Four reviewers evaluated all foci of bone marrow metastasis on 2-[^{18}F]FDG-PET and DW-MRI to assess concordance and measured the tumor-to-bone marrow contrast. Results were assessed with

Corresponding author: Heike E. Daldrup-Link, MD, PhD. H.E.Daldrup-Link@stanford.edu Department of Radiology, Lucile Packard Children's Hospital, Stanford University School of Medicine, 725 Welch Rd, Stanford, CA 94305-5654, Ph (lab): (650) 723-1127, fax: (650) 725-8957.

a one-sample Wilcoxon test and Generalized Estimation Equation. Bone marrow biopsies and follow-up imaging served as the standard of reference.

Results: The reviewers detected 884 (884/925, 95.5%) bone marrow metastases on 2-[^{18}F]FDG-PET and 893 (893/925, 96.5%) bone marrow metastases on DW-MRI. We found different "blind spots" for 2-[^{18}F]FDG-PET and MRI: 2-[^{18}F]FDG-PET missed sub-centimeter lesions while DW-MRI missed lesions in small bones. Sensitivity and specificity were 91.0% and 100% for ^{18}F-FDG-PET, 89.1% and 100.0% for DW-MRI, and 100.0% and 100.0% for combined modalities, respectively. The diagnostic accuracy of combined 2-[^{18}F]FDG-PET/MRI (100.0%) was significantly higher compared to either 2-[^{18}F]FDG-PET (96.9%, $p<0.001$) or DW-MRI (96.3%, $p<0.001$).

Conclusions: Both 2-[^{18}F]FDG-PET and DW-MRI can miss bone marrow metastases. The combination of both imaging techniques detected significantly more lesions than either technique alone.

Keywords

2-[^{18}F]FDG-PET; DW-MRI; PET/MRI; children; bone marrow metastases

Introduction

Bone or bone marrow metastases are present at initial diagnosis in up to 11% of children with rhabdomyosarcoma [1], 10% with Ewing sarcoma [2], and 8% with Hodgkin lymphoma [3]. The presence of bone and bone marrow metastases [4; 5] may require intensified therapy and is associated with poor overall survival. Historically, bone marrow aspirations and biopsies from the posterior superior iliac crest were used to diagnose bone marrow metastases in children with cancer [6; 7]. However, this painful procedure only samples a small area, leading to limited sensitivity [8]. Several studies showed improved sensitivities of 2-[^{18}F]fluoro-2-deoxy-D-glucose (2-[^{18}F]FDG) enhanced positron emission tomography (PET), because 2-[^{18}F]FDG-PET can sample the entire bone marrow [9; 10]. However, 2-[^{18}F]FDG-PET is not universally available due to logistic, technical or administrative/insurance coverage constraints. In addition, 2-[^{18}F]FDG-PET is associated with significant radiation exposure, especially when combined with computed tomography (CT) for anatomical co-registration of radiotracer data and for attenuation correction [11; 12].

More recently, ionizing radiation-free diffusion-weighted magnetic resonance imaging (DW-MRI) has been introduced for whole-body staging of adults [13; 14] and children [15; 16]. Whole-body DW-MRI sequences are part of the standard pulse sequence packages of all major MRI vendors. The application of these sequences does not require specific technical expertise of a technician, beyond the expertise of applying MRI sequences for imaging the bone marrow. However, adding Whole-body DW-MRI to a Whole-body MRI protocol adds additional time to the exam. Our data show, that this additional time can lead to the detection of additional lesions and is therefore well invested [15]. However, the diagnostic accuracy of DW-MRI for the detection of bone marrow metastases in children has not been systematically compared with that of 2-[^{18}F]FDG-PET.

In 16 adult patients with lymphoma, Asenbaum et al. reported sensitivities and specificities of DW-MRI of 100% and 90.9%, respectively, for the detection of focal bone marrow metastases and 87.5% and 56.8%, respectively, for the detection of diffuse bone marrow metastases [17]. Other investigators reported equal diagnostic accuracy of DW-MRI and 2-[^{18}F]FDG-PET for the detection of bone marrow metastases in 20 adult patients with thyroid cancer [18] and 25 adults with non-small cell lung cancer [19].

In children, Ishiguchi et al. reported sensitivities and specificities of DW-MRI of 94.7% and 24%, respectively, for the detection of bone marrow metastases in 13 patients with neuroblastoma [20].

Perhaps due to the low incidence of bone marrow metastases in children compared to adults, no systematic comparisons of DW-MRI and 2-[^{18}F]FDG-PET for the detection of bone marrow metastases in children exists to date. Closing this gap is important, because the diagnosis of bone marrow metastases has major implications for patient management. Therefore, with the hypothesis that DW-MRI and 2-[^{18}F]FDG-PET provide equal diagnostic accuracy for the detection of bone marrow metastases, the purpose of our study was to compare the diagnostic accuracy of DW-MRI and 2-[^{18}F]FDG-PET for the detection of bone marrow metastases in children and young adults.

Materials and Methods

Study design

This cross-sectional single-center study involved the analysis of a secondary aim of a prospective clinical trial (NCT01542879), which enrolled 108 children and young adults between May 2015 and July 2020. The study was conducted in compliance with the Declaration of Helsinki and the Health Insurance Portability and Accountability Act, and was approved by the institutional review board at Stanford University (IRB20221 and IRB44706). All patients or their legal representative gave written informed consent to undergo whole-body staging with integrated 2-[^{18}F]FDG-PET/MRI. To evaluate a secondary aim of determining the diagnostic accuracy of 2-[^{18}F]FDG-PET and DW-MRI for the detection of bone marrow metastases, we identified 23 patients from the initial cohort who had been diagnosed with one or more bone marrow metastases. The inclusion criteria were participation in the NCT01542879 clinical trial and one or more bone marrow metastases on any of their medical imaging scans for cancer staging (x-ray, CT, MRI, FDG-PET or bone scan). Exclusion criteria were major artifacts or incomplete imaging studies.

Simultaneous 2-[^{18}F]FDG-PET and DW-MRI

We used a PET/MRI scanner (3T Signa PET/MR, GE Healthcare) which allowed us to acquire sixty-six 2-[^{18}F]FDG-PET and DW-MRI scans simultaneously (23 baseline scans and 43 follow-up scans after chemotherapy), thereby excluding timing of the scans as a potential confounding variable. Due to technical issues in acquiring DW-MRI, one baseline scan was excluded. Therefore, 22 baseline scans were included for analysis (Fig. 1).

2-[^{18}F]FDG-PET: Patients were instructed to fast for at least 4 hours, as confirmed by their blood glucose level of <140 mg/dL. 2-[^{18}F]FDG was injected at a dose of 3 MBq/kg

bodyweight, followed whole-body PET scanning after an uptake time of 60 minutes. Axial PET acquisition slabs were obtained with a field of view (FOV) of 25 cm, and an acquisition time of 3:30 min. We reconstructed PET data using a 3D time of flight iterative ordered subsets expectation maximization algorithm (OSEM; 24 subsets, 3 iterations, matrix 192×192). The anatomic coverage in the z-direction for PET was 25 cm. 2-[^{18}F]FDG-PET scans were color encoded using a PET filter and fused with T1-weighted MR images using MIM software (version 6.5; MIM Software).

MRI: We obtained axial two-point Dixon sequences for attenuation correction of PET data (flip angle alpha = 5°, repetition time (TR) = 4.2 ms, echo time (TE) = 1.1, 2.3 ms), diffusion-weighted images with short tau inversion recovery (STIR) for fat suppression (TR=7824 ms, TE=56 ms, b-value= 50/800 sec/mm^2) and T1-weighted Liver Acquisition with Volume Acquisition (LAVA, alpha= 15°, TR=4364 ms, TE=1674 ms). LAVA scans for attenuation correction served as pre-contrast scans. Then, Gadavist was administered intravenously, followed by postcontrast LAVA sequences. The anatomic coverage in the z-direction for MRI was 50 cm. Using the OsiriX software (version 10.0, 64 bit; Pixmeo), the DW-MRI scans were color-encoded by applying a PET color filter and fused with T1-weighted LAVA images [15].

Qualitative and quantitative evaluation of bone marrow lesions

Two reviewers (H.E.D.L. and E.B.G. with >20 years and 6 years of experience, respectively, in interpreting whole-body MRI and FDG-PET scans) independently evaluated integrated 2-[^{18}F]FDG-PET/MR scans, composed of 2-[^{18}F]FDG-PET scans and contrast-enhanced MRI scans, in analogy to the clinical evaluation of a PET/CT scan. The reviewers also separately evaluated integrated DW-MRI scans, composed of DWI scans and contrast-enhanced MRI scans (Fig. 2). One reviewer started with the 2-[^{18}F]FDG-PET/MR scans and the other reviewer started with the DW-MRI scans. After an interval of at least three weeks, the reviewers evaluated the respective other imaging technology. All scans were evaluated for metastases detection. Both reviewers determined the presence or absence of bone marrow metastases in 10 anatomical regions per patient, according to a 5-point Likert scale (1-definitely absent – 5-definitely present). The evaluated anatomical regions included head, spine, ribs/clavicle, humerus, radius/ulna, hand, pelvis, femur, tibia/fibula, and foot. One reviewer (H.E.D.L.) also measured the size of up to 10 bone marrow lesions per anatomical region per patient on the MRI scans. According to the current clinical practice, we measured the size of the bone marrow lesions on the MRI scans as the lesion size is not typically measured on FDG-PET scans. The reviewers were blinded to clinical information. We eventually calculated the agreement of results obtained from both reviewers.

For quantitative analysis, a radiologist (A.J.T., 5 years of experience in interpreting whole-body MRI scans) measured the signal-to-noise ratio (SNR) of the largest bone lesion per anatomical region and normal bone marrow on DW-MRI through operator defined regions of interest (ROIs) [21; 22], using OsiriX software (version 10.0, 64 bit; Pixmeo). While we routinely acquire apparent diffusion coefficient (ADC) maps and made these available to the reviewers, ADC maps in children provide poor contrast between bone marrow lesions and bone marrow and therefore provide limited information for tumor detection.

Therefore, we used SNR for the quantitative evaluation of DW-MRI scans. Nevertheless, the ADC maps were available to reviewers. In addition, a nuclear medicine physician (L.B., 7 years of experience in interpreting whole-body FDG-PET scans) measured the maximum standardized uptake value (SUV_{max}) of the same bone marrow metastasis and the mean standardized uptake value (SUV_{mean}) of the normal bone marrow on 2-[^{18}F]FDG-PET scans, using MIM software (version 6.5; MIM Software). The quantitative measurements for normal bone marrow on DW-MRI and 2-[^{18}F]FDG-PET scans were performed on the same slice and adjacent to the bone marrow lesion. We calculated the contrast between bone marrow metastases (met) and normal bone marrow (BM):

$$\text{SNR metastasis to marrow contrast } (\%) = \frac{(SNR\ \ met - SNR\ \ BM)\ \times\ 100}{SNR\ \ BM}.$$

$$\text{SUV metastasis to marrow contrast } (\%) = \frac{(SUVmax\ \ met - SUVmean\ \ BM)\ \times\ 100}{SUVmean\ \ BM}.$$

Standard of reference

The combination of bone marrow aspiration/biopsy plus all other imaging studies (local MRI, CT, PET, whole-body MRI, bone scans) and follow-up imaging for at least six months served as the standard of reference for tumor detection in each patient and in each anatomical region. A positive bone marrow lesion on 2-[^{18}F]FDG-PET was defined as a focal lesion in the bone marrow with increased metabolic activity compared to the surrounding bone marrow. A positive bone marrow lesion on DW-MRI was defined as a focal lesion in the bone marrow with restricted diffusion compared to the surrounding bone marrow. A negative lesion was a lesion that was not positive, and an equivocal lesion was a lesion that was positive on one study and negative on another one. In case of equivocal imaging results with regards to the presence of a metastasis, a biopsy was obtained. The standard of reference for a viable lesion was interval growth on a follow up scan. Therefore, cancer therapy response was defined as follows: A bone marrow lesion that was stable in size or increased in size and/or number was defined as “non-responder”. A bone marrow lesion that decreased size or completely resolved was defined as “responder”.

Statistical Analysis

Power analyses—Based on 1000 simulations using a generalized linear mixed model (GLMM), a sample size of at least 20 patients with both 2-[^{18}F]FDG-PET and DW-MRI scans will provide 80.8% power (95% confidence interval [CI]: 78.22–83.20%) at 5% types I error to detect a difference of more than 1.5 standard deviations between scan types, considering one standard deviation (SD=1) of the random-intercept effect within each patient.

Data analyses—We first performed a “lesion-based” analysis to report the number of lesions that was detected on different imaging modalities. We next performed a “region-based” analysis, based on 10 regions per patient, to calculate the sensitivity, specificity, and diagnostic accuracy.

A one-sample Wilcoxon signed rank test was used to compare SUV and SNR values. A Generalized Estimation Equation (GEE) was used to correlate results of 2-[^{18}F]FDG-PET, DW-MRI and the standard of reference. All GEE models were adjusted for patient's age and gender. Sensitivities, specificities and diagnostic accuracies were computed using R package caret, and then compared between different modalities using GEE models. To evaluate the degree of agreement in Likert scale assessments between two reviewers, we calculated weighted kappa statistics [23; 24], using the kappa2() function from R package irr. Significant differences were considered for p-values of <0.05.

Results

Participant demographics

We investigated 925 bone marrow metastases in twenty-three patients (mean age, 16.8 years +/− 5.1 [SD]; range, 7–25 years; Fig. 1). These patients comprised 7 girls (16.9 years +/− 5.4; range, 7–25 years) and 16 boys (16.8 years +/− 5.1; range, 7–25 years; Table 1). Primary tumors included 13 bone or soft tissue sarcomas, 7 lymphomas (6 Hodgkin lymphoma and 1 non-Hodgkin lymphoma (NHL)), 2 carcinomas and one Wilms tumor. Twelve patients underwent 17 bone marrow biopsies from the iliac crest at baseline (n=12) and after treatment (n=5).

Diagnostic accuracy of 2-[^{18}F]FDG-PET and DW-MRI

2-[^{18}F]FDG-PET detected 884 bone marrow metastases (884/925, 95.5%), DW-MRI detected 893 bone marrow metastases (893/925, 96.5%) and combined scans detected 925 bone marrow metastases (925/925, 100.0%; Table 2). Combining 2-[^{18}F]FDG-PET and DW-MRI yielded a significantly higher number of detected bone marrow metastases compared to either scan alone (both p<0.001).

Considering all pre- and post-treatment scans, we found a sensitivity and specificity of 91.0% and 100.0% for 2-[^{18}F]FDG-PET, 89.1% and 100.0% for DW-MRI, and 100.0% and 100.0% for combined modalities, respectively (Table 3). The diagnostic accuracy of combined DW-MRI and 2-[^{18}F]FDG-PET (100.0%), was significantly higher compared to either 2-[^{18}F]FDG-PET (96.9%, p<0.001) or DW-MRI (96.3%, p<0.001) alone. There was a substantial inter-reader agreement for 2-[^{18}F]FDG-PET, DW-MRI, and integrated 2-[^{18}F]FDG-PET/MRI with a weighted kappa of 0.728, 0.770, and 0.767, respectively.

Detection of bone marrow metastases on baseline scans

At baseline, all bone marrow metastases demonstrated increased metabolic activity on 2-[^{18}F]FDG-PET scans and restricted diffusion on DW-MRI scans. All metastases that involved the bone cortex also involved the bone marrow. The SNR lesion to marrow contrast and SUV lesion to marrow contrast were not significantly different (p=0.53; Fig. 3).

According to the reference standard, our patients had 260 bone marrow metastases at baseline, of which 255 (255/260, 98.0%) were detected on 2-[^{18}F]FDG-PET and 250 (250/260, 96.1%) on DW-MRI (Table 2; p=0.29). Five lesions missed on 2-[^{18}F]FDG-PET included four subcentimeter lesions (Table 2, Supplemental Table 1) and one 1.5 cm lesion

with very low FDG uptake. Ten lesions missed on DW-MRI included lesions in small bones or areas with susceptibility artifacts (Fig. 4, Supplemental Table 2). We defined "small bones" as the ribs/clavicle, radius/ulna, and tibia/fibula. The small bones of the hands and feet would also fit into this category. However, our patients did not have any metastases in these bones (Supplemental Table 2). Sensitivities, specificities and diagnostic accuracies were 95.4%, 100.0% and 98.6%, respectively, for 2-[^{18}F]FDG-PET and 87.7%, 100.0% and 96.4%, respectively, for DW-MRI (p=0.20, p>0.99, p=0.14, respectively; Table 3). We found a comparable diagnostic accuracy of 2-[^{18}F]FDG-PET and DW-MRI for the detection of lesions in sarcomas. 2-[^{18}F]FDG-PET was more accurate than DW-MRI for the detection of bone marrow lesions in patients with lymphomas (Supplemental Table 3).

Detection of bone marrow metastases on post-treatment scans

On post-treatment scans, bone marrow metastases demonstrated variable changes: Three patients, two with lymphoma and one with choriocarcinoma, demonstrated therapy response. Twenty patients demonstrated disease progression. Five lymphoma lesions that demonstrated no MRI contrast enhancement at baseline now demonstrated contrast enhancement (Fig. 4). On post-treatment 2-[^{18}F]FDG-PET scans, the tumor SUV_{max} (5.2 +/− 4.5) decreased and the normal bone marrow SUV_{mean} increased (1.1 +/− 0.6). On post-treatment DW-MRI, the tumor SNR was highly variable (234.5 +/− 236.9), while the normal bone marrow SNR decreased (39.1 +/− 40.3, p<0.001). Accordingly, the lesion-to-marrow contrast was higher on post-treatment DW-MRI scans (794.4 +/− 721.9%) compared to 2-[^{18}F]FDG-PET scans (501.9 +/− 727.3%; p=0.06; Fig. 3).

According to the reference standard, our patients had 665 bone marrow metastases on post-treatment scans, of which 2-[^{18}F]FDG-PET detected 629 (629/665, 94.5%) and DW-MRI detected 643 (643/665, 96.6%; Table 2; p=0.08). Thirty-six lesions missed on 2-[^{18}F]FDG-PET included 23 subcentimeter lesions (23/36, 63.8%) and 13 lesions obscured by hypermetabolic bone marrow (13/36, 36.2%; Fig. 5). On DW-MRI, twenty-two missed lesions included lesions in small bones and areas affected by susceptibility artifacts. While 2-[^{18}F]FDG-PET was more accurate than DW-MRI for the detection of bone marrow lesions in small bones on both baseline and post-treatment scans, subcentimeter bone marrow lesions were better detected on post-treatment DW-MRI (Supplemental Table 4). Sensitivity, specificity and diagnostic accuracy were 89.1%, 100.0% and 96.0% for 2-[^{18}F]FDG-PET as well as 89.7%, 100.0% and 96.3% for DW-MRI, respectively (Table 3; all p>0.99). Thirteen of 665 bone marrow metastases demonstrated reduced metabolism on post-treatment 2-[^{18}F]FDG-PET and increasing size on post-treatment DW-MRI (Fig. 5). In all of these PET-negative cases, progressive disease was confirmed by interval growth on follow up scans or biopsy. These cases highlight the need to carefully follow presumed "treated" bone marrow lesions.

Discussion

Our data showed that both 2-[^{18}F]FDG-PET and DW-MRI can miss bone marrow metastases. However, the two exams had different "blind spots": 2-[^{18}F]FDG-PET missed subcentimeter lesions and lesions in reconverted hypermetabolic marrow while DW-MRI

missed lesions in small bones or areas with susceptibility artifacts. Therefore, the combination of 2-[^{18}F]FDG-PET and DW-MRI provided a higher diagnostic accuracy than either modality alone.

Several studies reported that 2-[^{18}F]FDG-PET has a higher sensitivity for the detection of bone marrow metastases compared to bone marrow biopsy because whole-body 2-[^{18}F]FDG-PET evaluates the entire bone marrow, while bone marrow aspirations only sample a small area [25; 26]. This led to replacement of bone marrow biopsies by whole-body 2-[^{18}F]FDG-PET scans for patients with Hodgkin lymphoma, who typically present with bone marrow disease in a focal and “spotty” pattern [26]. For patients with Ewing sarcomas, the most recent National Comprehensive Cancer Network (NCCN) guidelines currently suggests both 2-[^{18}F]FDG-PET and bone marrow biopsies for the evaluation of bone marrow disease [27]. However, a recently published study suggested that bone marrow biopsies can be omitted when whole-body 2-[^{18}F]FDG-PET is available [28]. Our data show that small subcentimeter metastases can be missed in these patients. This “blind spot” can be covered by simultaneous DW-MRI.

In patients with non-Hodgkin lymphomas (NHL), marrow involvement typically presents with a diffuse pattern which is more difficult to detect on imaging studies [29]. In these patients, bone marrow biopsy is important, specifically for distinguishing NHL with 6–25% blasts in the marrow and acute leukemia with >25% blasts in the bone marrow [30].

Similar to the above findings for whole-body 2-[^{18}F]FDG-PET scanning, several researchers reported a higher sensitivity of whole-body DW-MRI for the detection of bone marrow metastases compared to bone marrow biopsy [31; 32]. However, few studies compared the sensitivity of 2-[^{18}F]FDG-PET with that of DW-MRI. All of these studies were conducted in adult patients: Sun et al reported a sensitivity of 92.5% for 2-[^{18}F]FDG-PET and 93.0% for DW-MRI ($p>0.05$) for the diagnosis of bone marrow metastasis in 39 adults with lung, breast, prostate, and colon cancers [33]. Sakurai et al reported a sensitivity of 79.0% for 2-[^{18}F]FDG-PET and 82.0% for DW-MRI in 20 adults with thyroid cancer [18]. Lin et al found equal sensitivity of whole-body DW-MRI and 2-[^{18}F]FDG-PET/CT for staging of adults with diffuse large B-cell lymphoma [34].

Only one study by Ishiguchi et al compared the sensitivity and specificity of 2-[^{18}F]FDG-PET and DW-MRI in children with neuroblastoma who had 11 bone metastases [20]. Patients with neuroblastoma are typically staged with metaiodobenzylguanidine (MIBG) scans and it is not clear, if these results apply to children with lymphoma and sarcoma, who are typically older and undergo different therapies.

Since we evaluated patients with a larger number of 925 bone marrow metastases, we could consider several variables that might affect the performance of DW-MRI and 2-[^{18}F]FDG-PET, including status pre-/post-therapy, lesion location and lesion size. We found that 2-[^{18}F]FDG-PET can miss small bone marrow metastases. This challenges our current knowledge, as several previous studies assumed sensitivities and specificities of 100.0% for 2-[^{18}F]FDG-PET [10; 35]. In support of our finding, the limitation of 2-[^{18}F]FDG-PET to detect subcentimeter lesions in other organ systems such as the lungs [36] and lymph

nodes [37] has been well described. Importantly, we found different “blind spots” for DW-MRI: DW-MRI successfully detected subcentimeter lesions, but missed lesions in small bones, which were easily detected with 2-[^{18}F]FDG-PET. Therefore, a combination of both modalities should be considered. This could be easily achieved by simultaneous 2-[^{18}F]FDG-PET/MRI [38], but also by sequential scans [39].

We reported for the first time that bone marrow metastases with reduced metabolic activity on post-treatment 2-[^{18}F]FDG-PET can grow. Other authors described decreasing metabolic activity on 2-[^{18}F]FDG-PET and increasing tumor size on MRI in the context of pseudo-progression after immunotherapy in adult [40] and pediatric patients [41]. However, in our cases, the tumor growth noted on DW-MRI continued on follow-up scans, consistent with true tumor progression. We realize that we could have missed an interim tumor regression, which was eventually followed by true progression. However, if such interim regression occurred, it had no clinical impact.

In our study, all metastases that involved the bone cortex also involved the bone marrow, while not all marrow metastases involved the bone cortex. Thus, we conclude that bone metastases start in the bone marrow. This is in accordance with previous observations [42]. While primary malignant tumors [43] or metastatic bronchogenic carcinomas in adult patients [44] can start in the bone cortex, we did not find a reference that described the origin of a metastasis of a pediatric tumor in the bone cortex.

A positive bone marrow lesion on DW-MRI was defined as a focal lesion in the bone marrow with restricted diffusion compared to the surrounding bone marrow and increased signal compared to background tissues on high b-value DW images compared to low b-value images. Several studies described an increased signal of tumors compared to background tissues on high b-value DW images compared to low b-value images. It is because of the decreasing contribution of T2-effects to the tumor signal on DW images [45–47]. The ADC values of both lesion and normal bone marrow are high in children. Therefore, measuring ADC values is of limited value for the evaluation of bone marrow lesions in children due to the high cellularity of the normal bone marrow. However, the high b-value DW images typically show high tumor-to-background contrast, possibly due to intrinsic iron deposition in the normal bone marrow.

FDG hypermetabolic brown fat has been reported as a cause of false positive on FDG-PET scans, specifically in children [48], due to concealing small osteo-medullary metastases close to tissues with high brown fat content [49]. However, we did not encounter this problem on our PET/MR scans because the high soft tissue contrast, high anatomical resolution, and simultaneous data acquisition of FDG-PET and MRI scans could clearly delineate FDG metabolic activity in fat versus bone.

Similarly, we previously reported problems to localize FDG hypermetabolic lesions in neighboring tissues with normal high glucose metabolism on a PET scan [50]. This problem has markedly improved by using simultaneously acquired PET/MRI scans. In fact, we missed only one lesion in the skull on the PET and only one lesion in the skull on the MRI.

In this study, we followed the Society of Nuclear Medicine and Molecular Imaging (SNMMI) and The European Association of Nuclear Medicine (EANM) guidelines for using 2-[^{18}F]FDG in PET imaging of pediatric patients [51]. In adult patients with cancers, reducing the recommended dose of 2-[^{18}F]FDG radiotracer by 50% led to images of diagnostic quality for the diagnosis of bone metastases [52]. However, as such reduced radiotracer doses are not consistent with current clinical guidelines, we followed the most recent guidelines for using 2-[^{18}F]FDG in pediatric patients [51]. Nevertheless, the diagnostic image quality of PET/MR scans with lower 2-[^{18}F]FDG doses for the diagnosis of bone marrow metastases in children could be evaluated in future investigations.

Future approaches for the detection of bone marrow metastases might integrate liquid biopsies in staging and response assessment. Klega et al reported that circulating tumor deoxyribonucleic acid (DNA) can be used to detect tumor progression in children with solid tumors [53]. However, liquid biopsies cannot localize where the tumor progression is occurring. In addition, the circulating tumor DNA may remain detectable after irradiation therapy [53], which would be particularly significant for patients with bone marrow metastases.

We noted several limitations of our study: We included patients with a variety of different tumor types. Our goal was to investigate the performance of DW-MRI and 2-[^{18}F]FDG-PET in a patient cohort representative of patients typically referred for whole-body imaging in a major Children's Hospital. Bone metastases in children are rare. To our knowledge, we evaluated the largest population of children with bone metastases with integrated PET/MRI. We enrolled only patients with bone metastases in this study in order to evaluate various variables, such as location, size, primary tumor, and pre/post-treatment status on the ability of DW-MRI and 2-[^{18}F]FDG-PET to detect these lesions. By evaluating ten different anatomical regions per patient, we included areas that were negative for bone metastases and therefore could calculate negative predictive values. However, in clinical practice, we see many more patients that do not have bone metastases. Calculations of PPV and NPV might be different if considering larger groups of patients with and without bone metastases. Our whole-body imaging scans were obtained with free-breathing protocols. Sensitivities and specificities could potentially be improved with respiratory-gated imaging protocols. However, respiratory-gated sequences substantially increase overall scan time, which in our experience has more negative impact on overall scan quality. The insurance authorization for a PET/MR can add an additional layer of complexity. However, in our clinical practice, we successfully managed to replace all PET/CT scans of children with cancer by PET/MR scans. Furthermore, from a financial point of view, this can be particularly advantageous in young children where we can either reduce anesthesia time or replace two anesthesias (e.g., for a separate PET/CT and MRI) by one anesthesia for an integrated scan.

In summary, we found that both 2-[^{18}F]FDG-PET and DW-MRI can miss bone marrow metastases, although the "blind spot" of each modality is different. Therefore, combined 2-[^{18}F]FDG-PET and DW-MRI is the most precise modality for the diagnosis of bone marrow metastases in children and young adults.

Supplementary Material

Refer to Web version on PubMed Central for supplementary material.

Acknowledgements:

This work was in part supported by a grant from the Eunice Kennedy Shriver National Institute of Child Health and Human Development, grant number R01 HD081123.

Statistical analysis for this work was also partially supported by the Biostatistics Shared Resources, which is funded by the Cancer Center Support Grant, P30CA124435.

We thank Dawn Holley, Kim Halbert and Mehdi Khalighi from the PET/MRI Metabolic Service Center for their assistance with the acquisition of PET/MRI scans at the Lucas Research Center at Stanford. We thank Hasti Gholami for her help in the preparation of the Fig. 2. We thank the members of the Daldrup-Link lab for valuable input and discussions regarding this project.

Abbreviations

2-[^{18}F]FDG-PET	2-[^{18}F]fluoro-2-deoxy-D-glucose enhanced positron emission tomography
ADC	apparent diffusion coefficient
CI	confidence interval
CT	computed tomography
DNA	deoxyribonucleic acid
DWI	diffusion weighted imaging
EANM	European Association of Nuclear Medicine
FOV	field of view
GEE	Generalized Estimation Equation
GLMM	generalized linear mixed model
IRB	institutional review board
LAVA	Liver Acquisition with Volume Acquisition
MIBG	metaiodobenzylguanidine
MRI	magnetic resonance imaging
NCCN	National Comprehensive Cancer Network
NHL	non-Hodgkin lymphomas
OSEM	ordered subsets expectation maximization
ROI	regions of interest
SD	standard deviation

SNMMI	Society of Nuclear Medicine and Molecular Imaging
SNR	signal-to-noise ratio
SUV	standardized uptake value
TE	echo time
TR	repetition time

References

1. Weiss AR, Lyden ER, Anderson JR et al. (2013) Histologic and clinical characteristics can guide staging evaluations for children and adolescents with rhabdomyosarcoma: a report from the Children's Oncology Group Soft Tissue Sarcoma Committee. J Clin Oncol 31:3226–3232 [PubMed: 23940218]
2. Cotterill SJ, Ahrens S, Paulussen M et al. (2000) Prognostic factors in Ewing's tumor of bone: analysis of 975 patients from the European Intergroup Cooperative Ewing's Sarcoma Study Group. J Clin Oncol 18:3108–3114 [PubMed: 10963639]
3. Levis A, Pietrasanta D, Godio L et al. (2004) A large-scale study of bone marrow involvement in patients with Hodgkin's lymphoma. Clin Lymphoma 5:50–55 [PubMed: 15245608]
4. Oberlin O, Rey A, Lyden E et al. (2008) Prognostic factors in metastatic rhabdomyosarcomas: results of a pooled analysis from United States and European cooperative groups. J Clin Oncol 26:2384–2389 [PubMed: 18467730]
5. Paulussen M, Ahrens S, Burdach S et al. (1998) Primary metastatic (stage IV) Ewing tumor: survival analysis of 171 patients from the EICESS studies. European Intergroup Cooperative Ewing Sarcoma Studies. Ann Oncol 9:275–281 [PubMed: 9602261]
6. Balamuth NJ, Womer RB (2010) Ewing's sarcoma. Lancet Oncol 11:184–192 [PubMed: 20152770]
7. Cesari M, Righi A, Colangeli M et al. (2019) Bone marrow biopsy in the initial staging of Ewing sarcoma: Experience from a single institution. Pediatr Blood Cancer 66:e27653 [PubMed: 30724024]
8. Cheng G, Alavi A (2013) Value of 18F-FDG PET versus iliac biopsy in the initial evaluation of bone marrow infiltration in the case of Hodgkin's disease: a meta-analysis. Nucl Med Commun 34:25–31 [PubMed: 23111383]
9. Wang Y, Xie L, Tian R et al. (2019) PET/CT-based bone-marrow assessment shows potential in replacing routine bone-marrow biopsy in part of patients newly diagnosed with extranodal natural killer/T-cell lymphoma. J Cancer Res Clin Oncol 145:2529–2539 [PubMed: 31485768]
10. Yağci-Küpeli B, Koçyiğit-Deveci E, Adamhasan F, Küpeli S (2019) The Value of 18F-FDG PET/CT in Detecting Bone Marrow Involvement in Childhood Cancers. J Pediatr Hematol Oncol 41:438–441 [PubMed: 31033787]
11. Kaushik A, Jaimini A, Tripathi M et al. (2015) Estimation of radiation dose to patients from (18) FDG whole body PET/CT investigations using dynamic PET scan protocol. Indian J Med Res 142:721–731 [PubMed: 26831421]
12. Chawla SC, Federman N, Zhang D et al. (2010) Estimated cumulative radiation dose from PET/CT in children with malignancies: a 5-year retrospective review. Pediatr Radiol 40:681–686 [PubMed: 19967534]
13. Kharuzhyk S, Zhavrid E, Dziuban A, Sukolinskaja E, Kalenik O (2020) Comparison of whole-body MRI with diffusion-weighted imaging and PET/CT in lymphoma staging. Eur Radiol 30:3915–3923 [PubMed: 32103366]
14. Soydan L, Demir AA, Torun M, Cikrikcioglu MA (2020) Use of Diffusion-Weighted Magnetic Resonance Imaging and Apparent Diffusion Coefficient in Gastric Cancer Staging. Curr Med Imaging 16:1278–1289 [PubMed: 32108000]

15. Klenk C, Gawande R, Uslu L et al. (2014) Ionising radiation-free whole-body MRI versus (18)F-fluorodeoxyglucose PET/CT scans for children and young adults with cancer: a prospective, non-randomised, single-centre study. Lancet Oncol 15:275–285 [PubMed: 24559803]
16. Regacini R, Puchnick A, Luisi FAV, Lederman HM (2018) Can diffusion-weighted whole-body MRI replace contrast-enhanced CT for initial staging of Hodgkin lymphoma in children and adolescents? Pediatr Radiol 48:638–647 [PubMed: 29362839]
17. Asenbaum U, Nolz R, Karanikas G et al. (2018) Bone Marrow Involvement in Malignant Lymphoma: Evaluation of Quantitative PET and MRI Biomarkers. Acad Radiol 25:453–460 [PubMed: 29199055]
18. Sakurai Y, Kawai H, Iwano S, Ito S, Ogawa H, Naganawa S (2013) Supplemental value of diffusion-weighted whole-body imaging with background body signal suppression (DWIBS) technique to whole-body magnetic resonance imaging in detection of bone metastases from thyroid cancer. J Med Imaging Radiat Oncol 57:297–305 [PubMed: 23721138]
19. Takenaka D, Ohno Y, Matsumoto K et al. (2009) Detection of bone metastases in non-small cell lung cancer patients: comparison of whole-body diffusion-weighted imaging (DWI), whole-body MR imaging without and with DWI, whole-body FDG-PET/CT, and bone scintigraphy. J Magn Reson Imaging 30:298–308 [PubMed: 19629984]
20. Ishiguchi H, Ito S, Kato K et al. (2018) Diagnostic performance of (18)F-FDG PET/CT and whole-body diffusion-weighted imaging with background body suppression (DWIBS) in detection of lymph node and bone metastases from pediatric neuroblastoma. Ann Nucl Med 32:348–362 [PubMed: 29667143]
21. Park C, Lee E, Yeo Y et al. (2018) Spine MR images in patients with pedicle screw fixation: Comparison of conventional and SEMAC-VAT sequences at 1.5 T. Magn Reson Imaging 54:63–70 [PubMed: 30099060]
22. Guo H, Lan S, He Y, Tiheiran M, Liu W (2021) Differentiating brucella spondylitis from tuberculous spondylitis by the conventional MRI and MR T2 mapping: a prospective study. Eur J Med Res 26:125 [PubMed: 34711265]
23. Cohen J (1968) Weighted kappa: nominal scale agreement with provision for scaled disagreement or partial credit. Psychol Bull 70:213–220 [PubMed: 19673146]
24. Landis JR, Koch GG (1977) The measurement of observer agreement for categorical data. Biometrics 33:159–174 [PubMed: 843571]
25. Cheng G, Chen W, Chamroonrat W, Torigian DA, Zhuang H, Alavi A (2011) Biopsy versus FDG PET/CT in the initial evaluation of bone marrow involvement in pediatric lymphoma patients. Eur J Nucl Med Mol Imaging 38:1469–1476 [PubMed: 21505896]
26. Purz S, Mauz-Körholz C, Körholz D et al. (2011) [18F]Fluorodeoxyglucose positron emission tomography for detection of bone marrow involvement in children and adolescents with Hodgkin's lymphoma. J Clin Oncol 29:3523–3528 [PubMed: 21825262]
27. Biermann JS, Chow W, Reed DR et al. (2017) NCCN Guidelines Insights: Bone Cancer, Version 2.2017. J Natl Compr Canc Netw 15:155–167 [PubMed: 28188186]
28. Kasalak Ö, Glaudemans A, Overbosch J, Jutte PC, Kwee TC (2018) Can FDG-PET/CT replace blind bone marrow biopsy of the posterior iliac crest in Ewing sarcoma? Skeletal Radiol 47:363–367 [PubMed: 29124298]
29. Chen S, Wang S, He K, Ma C, Fu H, Wang H (2018) PET/CT predicts bone marrow involvement in paediatric non-Hodgkin lymphoma and may preclude the need for bone marrow biopsy in selected patients. Eur Radiol 28:2942–2950 [PubMed: 29383519]
30. McCarten KM, Nadel HR, Shulkin BL, Cho SY (2019) Imaging for diagnosis, staging and response assessment of Hodgkin lymphoma and non-Hodgkin lymphoma. Pediatr Radiol 49:1545–1564 [PubMed: 31620854]
31. Albano D, Patti C, Lagalla R, Midiri M, Galia M (2017) Whole-body MRI, FDG-PET/CT, and bone marrow biopsy, for the assessment of bone marrow involvement in patients with newly diagnosed lymphoma. J Magn Reson Imaging 45:1082–1089 [PubMed: 27603267]
32. Balbo-Mussetto A, Saviolo C, Fornari A et al. (2017) Whole body MRI with qualitative and quantitative analysis of DWI for assessment of bone marrow involvement in lymphoma. Radiol Med 122:623–632 [PubMed: 28421406]

33. Sun W, Li M, Gu Y, Sun Z, Qiu Z, Zhou Y (2020) Diagnostic Value of Whole-Body DWI With Background Body Suppression Plus Calculation of Apparent Diffusion Coefficient at 3 T Versus (18)F-FDG PET/CT for Detection of Bone Metastases. AJR Am J Roentgenol 214:446–454 [PubMed: 31799866]
34. Lin C, Luciani A, Itti E et al. (2010) Whole-body diffusion-weighted magnetic resonance imaging with apparent diffusion coefficient mapping for staging patients with diffuse large B-cell lymphoma. Eur Radiol 20:2027–2038 [PubMed: 20309558]
35. Badr S, Kotb M, Elahmadawy MA, Moustafa H (2018) Predictive Value of FDG PET/CT Versus Bone Marrow Biopsy in Pediatric Lymphoma. Clin Nucl Med 43:e428–e438 [PubMed: 30358625]
36. Kernstine KH, Grannis FW Jr., Rotter AJ (2005) Is there a role for PET in the evaluation of subcentimeter pulmonary nodules? Semin Thorac Cardiovasc Surg 17:110–114 [PubMed: 16087077]
37. Muehe AM, Siedek F, Theruvath AJ et al. (2020) Differentiation of benign and malignant lymph nodes in pediatric patients on ferumoxytol-enhanced PET/MRI. Theranostics 10:3612–3621 [PubMed: 32206111]
38. Hirsch FW, Sattler B, Sorge I et al. (2013) PET/MR in children. Initial clinical experience in paediatric oncology using an integrated PET/MR scanner. Pediatr Radiol 43:860–875 [PubMed: 23306377]
39. Sher AC, Seghers V, Paldino MJ et al. (2016) Assessment of Sequential PET/MRI in Comparison With PET/CT of Pediatric Lymphoma: A Prospective Study. AJR Am J Roentgenol 206:623–631 [PubMed: 26901021]
40. Danylesko I, Shouval R, Shem-Tov N et al. (2020) Immune imitation of tumor progression after anti-CD19 chimeric antigen receptor T cells treatment in aggressive B-cell lymphoma. Bone Marrow Transplant. 10.1038/s41409-020-01156-y
41. Huang J, Rong L, Wang E, Fang Y (2021) Pseudoprogression of extramedullary disease in relapsed acute lymphoblastic leukemia after CAR T-cell therapy. Immunotherapy 13:5–10 [PubMed: 33045890]
42. Høilund-Carlsen PF, Hess S, Werner TJ, Alavi A (2018) Cancer metastasizes to the bone marrow and not to the bone: time for a paradigm shift! Eur J Nucl Med Mol Imaging 45:893–897 [PubMed: 29468310]
43. Van der Woude HJ, Hazelbag HM, Bloem JL, Taminiau AH, Hogendoorn PC (2004) MRI of adamantinoma of long bones in correlation with histopathology. AJR Am J Roentgenol 183:1737–1744 [PubMed: 15547221]
44. Greenspan A, Norman A (1988) Osteolytic cortical destruction: an unusual pattern of skeletal metastases. Skeletal Radiol 17:402–406 [PubMed: 3238438]
45. Padhani AR, van Ree K, Collins DJ, D'Sa S, Makris A (2013) Assessing the relation between bone marrow signal intensity and apparent diffusion coefficient in diffusion-weighted MRI. AJR Am J Roentgenol 200:163–170 [PubMed: 23255758]
46. Koh DM, Collins DJ (2007) Diffusion-weighted MRI in the body: applications and challenges in oncology. AJR Am J Roentgenol 188:1622–1635 [PubMed: 17515386]
47. Rezaeian A, Tahmasebi Birgani MJ, Chegeni N, Sarkarian M, Hanafi MGh, Akbarizadeh Gh(2019) Signal Intensity of High B-value Diffusion-weighted Imaging for the Detection of Prostate Cancer. J Biomed Phys Eng 9:453–458 [PubMed: 31531298]
48. Truong MT, Erasmus JJ, Munden RF et al. (2004) Focal FDG uptake in mediastinal brown fat mimicking malignancy: a potential pitfall resolved on PET/CT. AJR Am J Roentgenol 183:1127–1132 [PubMed: 15385319]
49. Yeung HW, Grewal RK, Gonen M, Schöder H, Larson SM (2003) Patterns of (18)F-FDG uptake in adipose tissue and muscle: a potential source of false-positives for PET. J Nucl Med 44:1789–1796 [PubMed: 14602861]
50. Daldrup-Link HE, Franzius C, Link TM et al. (2001) Whole-body MR imaging for detection of bone metastases in children and young adults: comparison with skeletal scintigraphy and FDG PET. AJR Am J Roentgenol 177:229–236 [PubMed: 11418435]
51. Vali R, Alessio A, Balza R et al. (2021) SNMMI Procedure Standard/EANM Practice Guideline on Pediatric (18)F-FDG PET/CT for Oncology 1.0. J Nucl Med 62:99–110 [PubMed: 33334912]

52. Ohnona J, Michaud L, Balogova S et al. (2013) Can we achieve a radionuclide radiation dose equal to or less than that of 99mTc-hydroxymethane diphosphonate bone scintigraphy with a low-dose 18F-sodium fluoride time-of-flight PET of diagnostic quality? Nucl Med Commun 34:417–425 [PubMed: 23470463]

53. Klega K, Imamovic-Tuco A, Ha G et al. (2018) Detection of Somatic Structural Variants Enables Quantification and Characterization of Circulating Tumor DNA in Children With Solid Tumors. JCO Precis Oncol 2018

Key points

- DW-MRI and 2-[^{18}F]FDG-PET have different strengths and limitations for the detection of bone marrow metastases in children and young adults with solid tumors.
- Both modalities can miss bone marrow metastases, although the “blind spot” of each modality is different.
- A combined PET/MR imaging approach will achieve maximum sensitivity and specificity for the detection of bone marrow metastases in children with solid tumors.

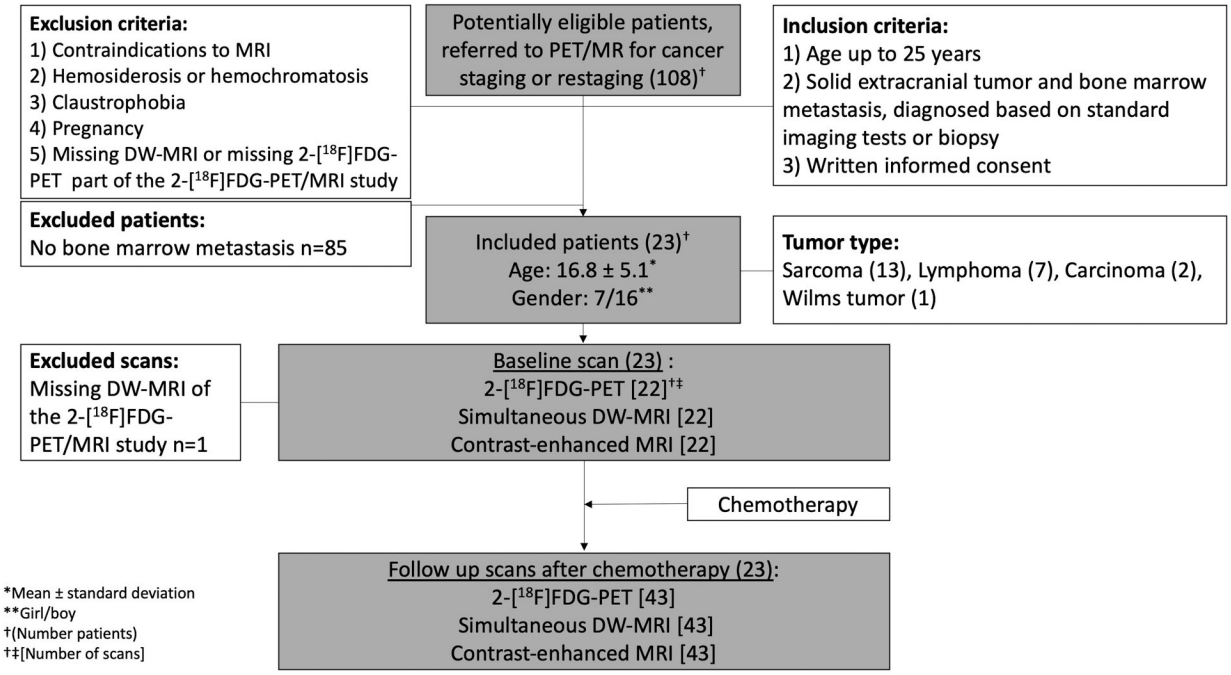

Fig. 1.

Flowchart of study design. Among 108 potentially eligible patients who were referred to PET/MR for cancer staging or restaging, 23 patients included in the study and underwent simultaneous 2-[^{18}F]FDG-PET, DW-MRI scan, and contrast-enhanced MRI. At baseline, 22 simultaneous 2-[^{18}F]FDG-PET, DW-MRI, and contrast-enhanced MRI scans were included. Following the chemotherapy treatment, 43 simultaneous 2-[^{18}F]FDG-PET, DW-MRI, and contrast-enhanced MRI scans were performed on the included patients.

Abbreviations: PET/MR: positron emission tomography/magnetic resonance, 2-[^{18}F]FDG-PET: 2-[^{18}F]fluoro-2-deoxy-D-glucose enhanced positron emission tomography, DW-MRI: Diffusion weighted-magnetic resonance imaging.

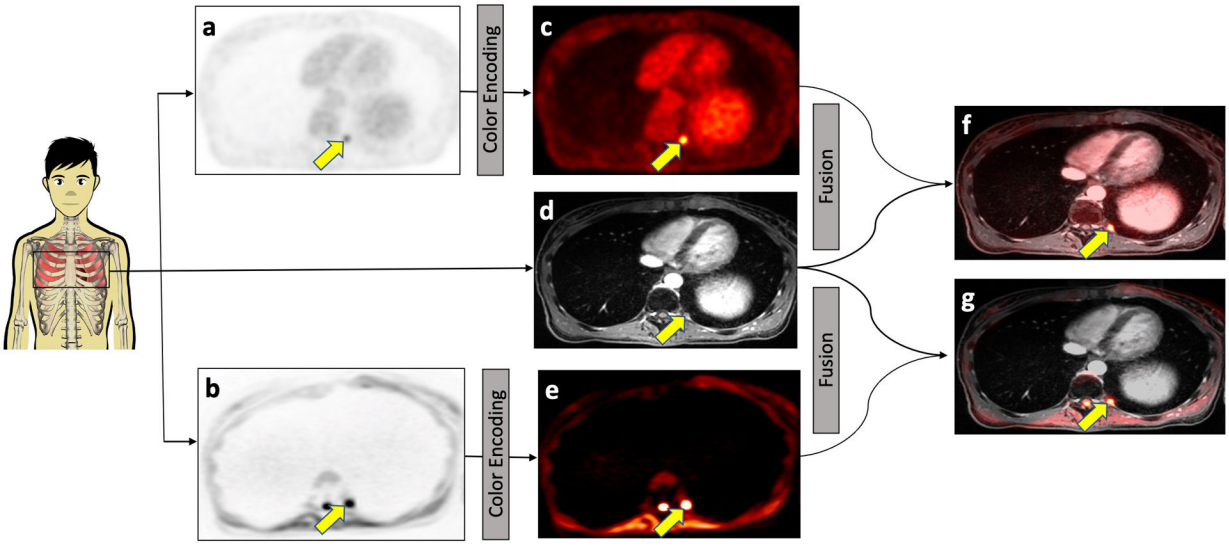

Fig. 2.

Concept of integrated 2-[^{18}F]FDG-PET/MRI and DW-MRI. 2-[^{18}F]FDG-PET (**a**) and DW-MRI (**b**) images were color-encoded (**c** and **e**, respectively) and then fused with the contrast-enhanced MRI scan (**d**) for anatomical orientation, yielding the integrated 2-[^{18}F]FDG-PET/MRI (**f**) or DW-MRI (**g**). Both 2-[^{18}F]FDG-PET and DW-MRI images visualize a subcentimeter bone marrow metastasis in the left proximal 11th rib (arrow) in a 25-year-old female patent with Wilms tumor.

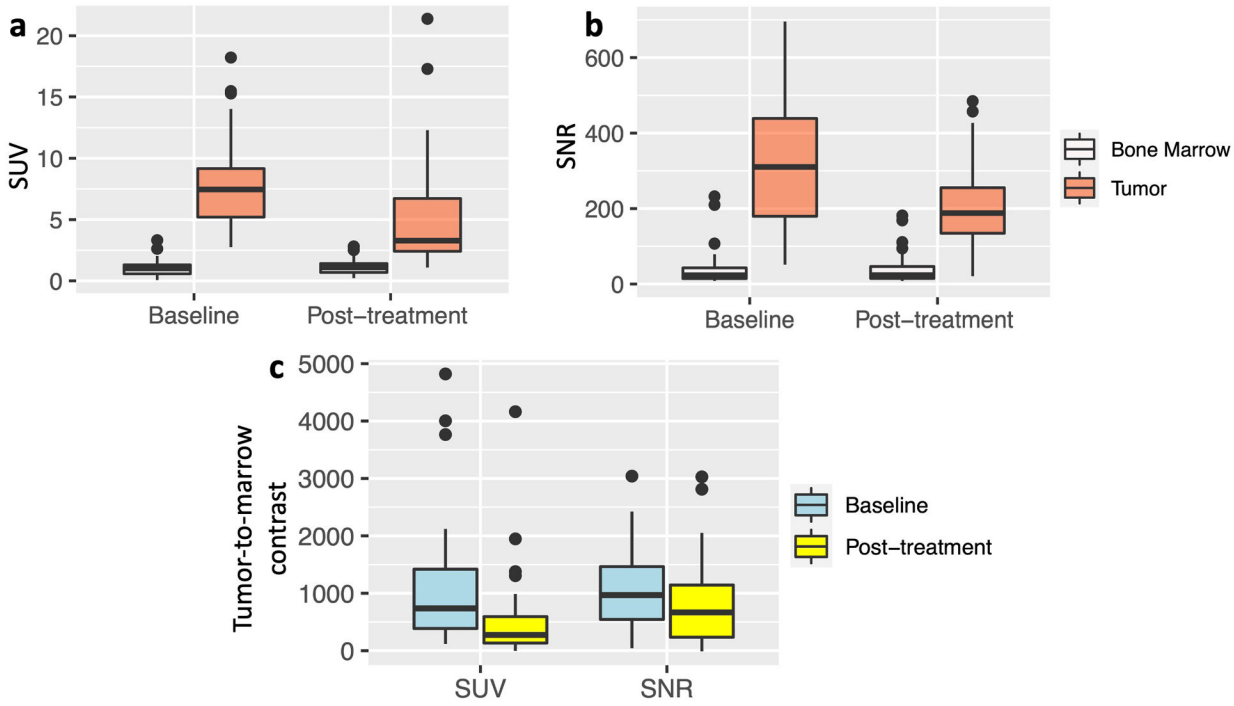

Fig. 3.

Quantitative evaluation of the tumor-to-marrow contrast on 2-[^{18}F]FDG-PET and DW-MRI scans. **a** 2-[^{18}F]FDG-PET: Standardized uptake values (SUV) of bone marrow metastases (SUV_{max}) are significantly higher compared to SUV_{mean} of normal bone marrow on baseline and post-treatment scans ($p < 0.001$, respectively). **b** DW-MRI: Signal-to-noise ratios (SNR) of bone marrow metastases (tumor) are significantly higher compared to SNR of normal bone marrow on baseline and post-treatment scans ($p < 0.001$, respectively). **c** The tumor-to-marrow contrast on 2-[^{18}F]FDG-PET, measured as the difference between the tumor SUV_{max} and normal bone marrow SUV_{mean}, was significantly smaller on post-treatment scans compared to baseline scans ($p=0.014$). The tumor-to-marrow contrast on DW-MRI, measured as the difference between the tumor SNR and normal bone marrow SNR, was not statistically significant between baseline and post-treatment scans ($p=0.118$). Baseline data are displayed as mean values of 62 true positive lesions on 2-[^{18}F]FDG-PET and 57 true positive lesions on DW-MRI plus standard deviations. Post-treatment data are displayed as mean values of 139 true positive lesions on 2-[^{18}F]FDG-PET and 140 true positive lesions on DW-MRI plus standard deviations.

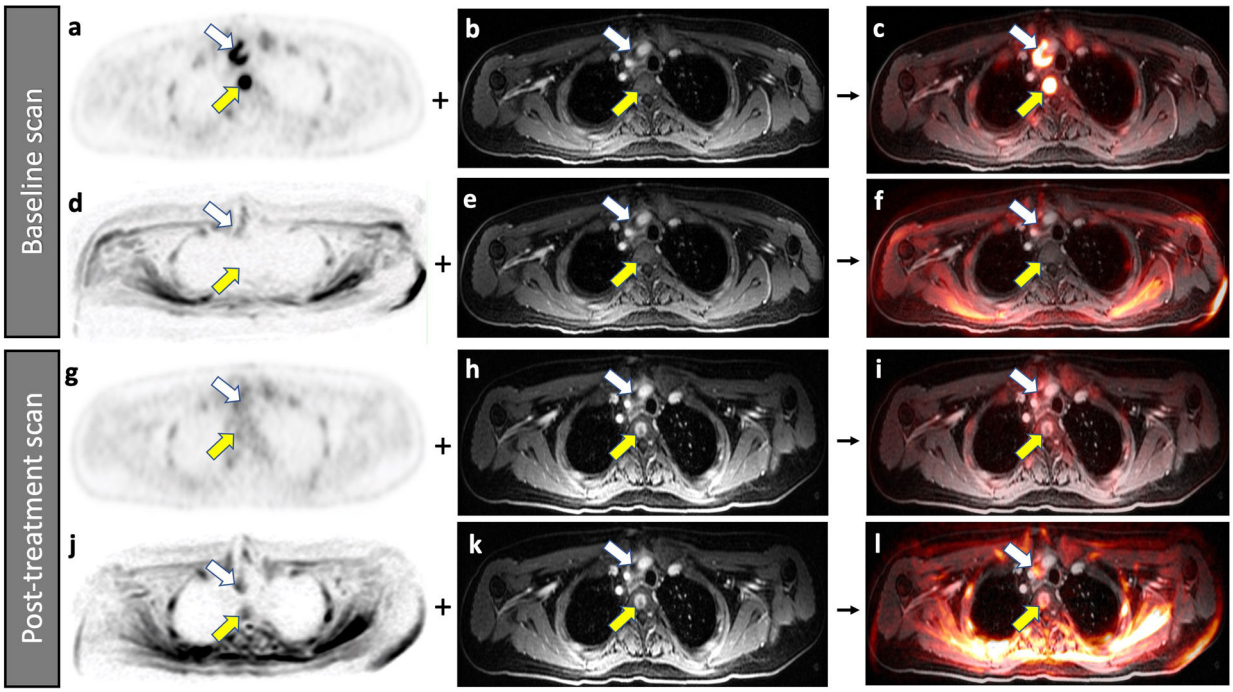

Fig. 4.

Improved detection of a bone marrow metastasis in a 22-year-old male patient with diffuse large B-cell lymphoma on 2-[^{18}F]FDG-PET compared to DW-MRI. **Baseline scans (a-f)**, A bone marrow metastasis in the third thoracic vertebra (yellow arrow) demonstrates high FDG uptake on 2-[^{18}F]FDG-PET (**a**). The lesion is not visible on the contrast enhanced MRI (**b**). The combined 2-[^{18}F]FDG-PET/MR scan localized the lesion to the vertebral body (**c**). The simultaneously acquired DW-MRI does not show the bone lesion because of local susceptibility artifacts (**d**). The lesion is also not visible on the contrast enhanced MRI (**e**). Therefore, the combined DW-MRI scan does not show the lesion either **(f)**. **Follow up scans after 2 weeks of chemotherapy (g-l)**, The bone marrow lesion demonstrates decreased FDG uptake on the 2-[^{18}F]FDG-PET scan (**g**), consistent with therapy response. The lesion now demonstrates contrast enhancement on the gadolinium chelate enhanced MRI scan (**h**), a typical feature of treated bone marrow lesions in patients with lymphoma. The lesion can be detected on the integrated 2-[^{18}F]FDG-PET/MRI scan (**i**). The simultaneously acquired DW-MRI (**j)** now shows the bone lesion as an area of restricted diffusion (yellow arrow). When fused with the gadolinium chelate enhanced MRI scan (**k**), the lesion can be equally well detected as on the integrated DW-MRI scan (**l**). Note that the patient also has a mediastinal lymph node (white arrow).

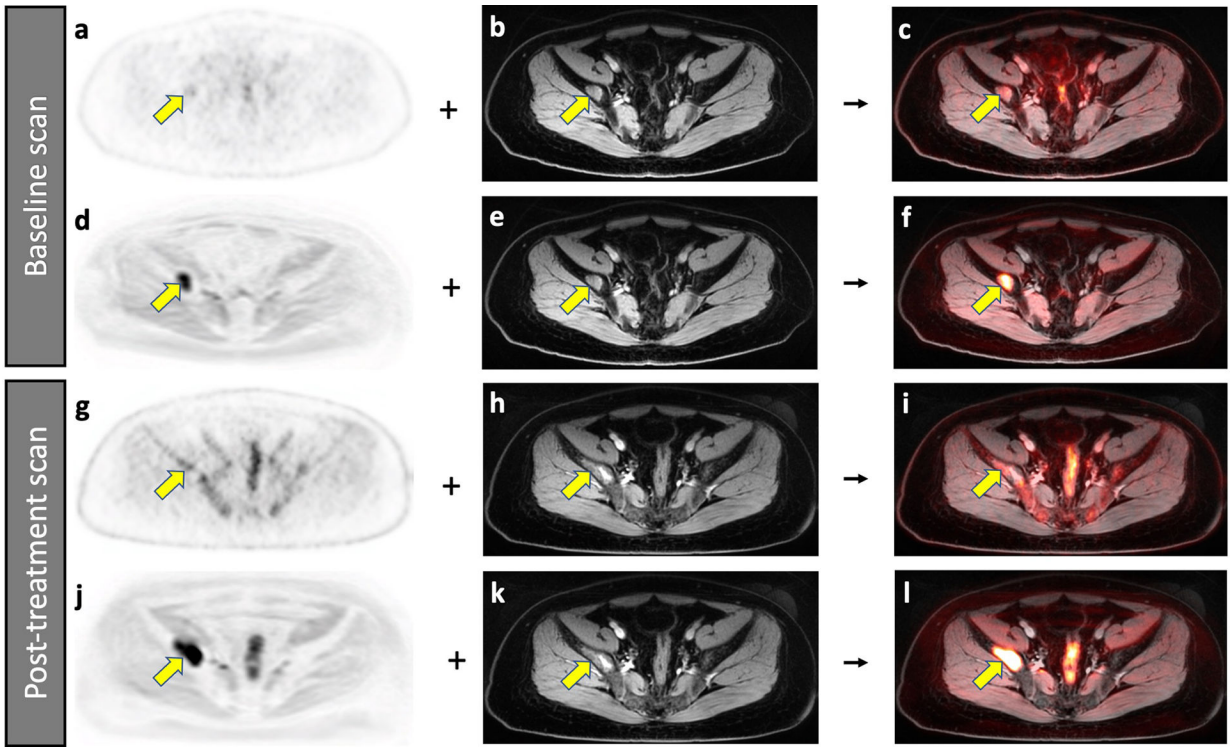

Fig. 5.

Improved detection of a bone marrow metastasis in an 18-year-old male patient with Ewing sarcoma on DW-MRI compared to 2-[^{18}F]FDG-PET scan. **Baseline scans (a-f)**, A bone marrow metastasis in the right iliac wing (arrow) demonstrates minor 2-[^{18}F]FDG uptake on the PET scan (**a**). The lesion is also noted on the contrast-enhanced T1-weighted gradient echo scan (**b**) and the integrated 2-[^{18}F]FDG-PET/MRI (**c**). The same bone marrow metastasis (arrow) demonstrates markedly restricted diffusion on the DW-MRI (**d**). After fusion with the contrast-enhanced MRI (**e**), it is better depicted on the integrated DW-MRI (**f**) than on the integrated 2-[^{18}F]FDG-PET/MR scan. **Follow up scans after 9 weeks of chemotherapy (g-l)**, On the post-treatment 2-[^{18}F]FDG-PET scan (**g**), the normal bone marrow demonstrates increased hypermetabolic activity, which obscures the lesion (yellow arrow). The contrast-enhanced MRI demonstrates a larger area of inhomogeneous enhancement (**h**). It is difficult to determine a change in size or metabolic activity based on the integrated 2-[^{18}F]FDG-PET/MRI (**i**). However, the DW-MRI scan (**j**) clearly demonstrates that the lesion increased in size. After fusion with the contrast-enhanced MRI (**k**), the integrated DW-MRI clearly demonstrates interval tumor growth (**l**). This case demonstrates that DW-MRI can sometimes better depict tumor progression than 2-[^{18}F]FDG-PET.

Table 1.

Participant demographics

Characteristic	Value (%)
Age (Year)	
Mean ± standard deviation	16.8 ± 5.1
Range	7–25
Sex [n =23]	
Female	7 (30.0)
Male	16 (70.0)
Diagnosis (tumor type) [n = 23]	
Sarcoma	13 (56.5)
Ewing sarcoma	7
Osteosarcoma	3
Rhabdomyosarcoma	2
Desmoplastic small round cell tumor	1
Lymphoma	7 (30.0)
Hodgkin lymphoma	6
Non-Hodgkin lymphoma	1
Carcinoma	2 (9.0)
Choriocarcinoma	1
Large cell neuroendocrine carcinoma	1
Wilms tumor	1 (4.5)
Scans, treatment status [n = 65]	
Baseline	22 (34.0)
Post-treatment	43 (66.0)
Bone marrow biopsy [n = 17]	
Baseline	12 (70.0)
Post-treatment	5 (30.0)

Table 2.

Number of bone marrow metastases, detected on 2-[^{18}F]FDG-PET-MRI, DW-MRI or combined scans.

Bone marrow lesions	Image modality	Total [% of detected lesions]	Baseline [% of detected lesions]	Post-treatment [% of detected lesions]
< 5 mm	2-[^{18}F]FDG-PET-MRI	111 [91.7%]	25 [100.0%]	86 [89.5%]
	DW-MRI	111 [91.7%]	20 [80.0%]	91 [94.7%]
	Combined	121 [100.0%]	25 [100.0%]	96 [100.0%]
	Standard of Reference	121 [100.0%]	25 [100.0%]	96 [100.0%]
5–10 mm	2-[^{18}F]FDG-PET-MRI	280 [94.2%]	81 [95.2%]	199 [93.8%]
	DW-MRI	279 [93.9%]	82 [96.4%]	197 [92.9%]
	Combined	297 [100.0%]	85 [100.0%]	212 [100.0%]
	Standard of Reference	297 [100.0%]	85 [100.0%]	212 [100.0%]
>10 mm	2-[^{18}F]FDG-PET-MRI	493 [97.2%]	149 [99.3%]	344 [96.3%]
	DW-MRI	503 [99.2%]	148 [98.6%]	355 [99.4%]
	Combined	507 [100.0%]	150 [100.0%]	357 [100.0%]
	Standard of Reference	507 [100.0%]	150 [100.0%]	357 [100.0%]
All Lesions	2-[^{18}F]FDG-PET-MRI	884 [95.5%]	255 [98.0%]	629 [94.5%]
	DW-MRI	893 [96.5%][a]	250 [96.1%][a]	643 [96.6%][a]
	Combined	925 [100.0%][b]	260 [100.0%][b]	665 [100.0%][b]
	Standard of Reference	925 [100.0%]	260 [100.0%]	665 [100.0%]

[a]No statistically significant difference when comparing with 2-[^{18}F]FDG-PET-MRI ($p>0.05$).

[b]Statistically significant difference when comparing with either 2-[^{18}F]FDG-PET-MRI or DW-MRI ($p<0.001$).

Abbreviations: 2-[^{18}F]FDG-PET-MRI: 2-[^{18}F]fluoro-2-deoxy-D-glucose enhanced positron emission tomography-magnetic resonance imaging, DW-MRI: Diffusion weighted-magnetic resonance imaging

Table 3.

Diagnosis of bone marrow metastases on 2-[^{18}F]FDG-PET-MRI, DW-MRI or combined scans, based on reviewer assignments of 650 anatomical regions (10 regions per patient and imaging exam) as either positive or negative for tumor.

Treatment Status	Image modality	TP	FN	FP	TN	Sensitivity (%)	Specificity (%)	PPV (%)	NPV (%)	Accuracy (%)
Baseline	2-[^{18}F]FDG-PET-MRI	62	3	0	155	95.4	100.0	100.0	98.1	98.6
	DW-MRI	57	8	0	155	87.7[a]	100.0	100.0	95.1	96.4[a]
	Combined	65	0	0	155	100.0[b]	100.0	100.0	100.0	100.0[b]
	Standard of Reference	65	0	0	155	100.0	100.0	100.0	100.0	100.0
Post-treatment	2-[^{18}F]FDG-PET-MRI	139	17	0	274	89.1	100.0	100.0	94.2	96.0
	DW-MRI	140	16	0	274	89.7[a]	100.0	100.0	94.5	96.3[a]
	Combined	156	0	0	274	100.0[b]	100.0	100.0	100.0	100.0[b]
	Standard of Reference	156	0	0	274	100.0	100.0	100.0	100.0	100.0
All Lesions	2-[^{18}F]FDG-PET-MRI	201	20	0	429	91.0	100.0	100.0	95.5	96.9
	DW-MRI	197	24	0	429	89.1[a]	100.0	100.0	94.7	96.3[a]
	Combined	221	0	0	429	100.0[b]	100.0	100.0	100.0	100.0[b]
	Standard of Reference	221	0	0	429	100.0	100.0	100.0	100.0	100.0

[a]No statistically significant difference when comparing with 2-[^{18}F]FDG-PET-MRI ($p>0.05$).

[b]Statistically significant difference when comparing with either 2-[^{18}F]FDG-PET-MRI or DW-MRI ($p<0.001$).

Abbreviations: 2-[^{18}F]FDG-PET-MRI: 2-[^{18}F]fluoro-2-deoxy-D-glucose enhanced positron emission tomography-magnetic resonance imaging, DW-MRI: Diffusion weighted-magnetic resonance imaging, TP: true positive, FN: false negative, FP: false positive, TN: true negative, PPV: positive predictive value, NPV: negative predictive value.